Theoretical Mechanistic Study on the Radical−Radical Reaction of Ketenyl with Nitrogen Dioxide

Jia-xu Zhang, Ze-sheng Li,* Jing-yao Liu, and Chia-Chung Sun

Institute of Theoretical Chemistry, State Key Laboratory of Theoretical and Computational Chemistry, Jilin University, Changchun 130023, P.R. China

Received: November 13, 2005; In Final Form: January 1, 2006

The radical−radical reaction between the ketenyl radical (HCCO) and nitrogen dioxide (NO_2) played a very important role in atmospheric and combustion chemistry. Motivated by recent laboratory characterization about the reaction kinetics of ketenyl radical with nitrogen dioxide, in this contribution, we applied the coupled cluster and density functional theory to explore the mechanism of the title reaction. These calculations indicate that the title reaction proceeds mostly through singlet pathways, less go through triplet pathways. It is found that the HCCO + NO_2 reaction initially favors formation of adduct $OCCHNO_2$ (**1**) with no barrier. Subsequently, starting from isomer **1**, the most feasible pathway is ring closure of **1** to isomer O-cCCHN(O)O (**2**) followed by CO_2 extrusion to product HCNO + CO_2 ($\mathbf{P}_1$), which is the major product with predominant yields. Much less competitively, **1** can take the successive 1,3-H- and 1,3-OH-shift interconversion to isomer OCCNOHO (**3**[a], **3**[b], **3**[c]) and then to isomer OCOHCNO (**4**[a], **4**[b]), which can finally take a concerted H-shift and C−C bond fission to give HCNO + CO_2 ($\mathbf{P}_1$). The least competitive pathway is the ring-closure of isomer **3**[a] to form isomer O-cCCN(OH)O (**5**[a], **5**[b]) followed by dissociation to HONC + CO_2 ($\mathbf{P}_2$) through the direct side CO_2 elimination. Because the intermediates and transition states involved in the most favorable channel all lie below the reactants, the title reaction is expected to be rapid, as is confirmed by experiment. Therefore, it can be significant for elimination of nitrogen dioxide pollutants. The present results can lead us to a deep understanding of the mechanism of the title reaction and can be helpful for understanding NO_x-combustion chemistry.

1. Introduction

The spectroscopy[1−4] and kinetics[5−14] of the ketenyl radical (HCCO) is of interest, partly because it is important in combustion chemistry. It is of great significance to learn the behavior of the ketenyl radical for environmental protection. HCCO is formed in flames primarily by the oxidation of acetylene.[15,16] It has been observed in laboratory studies by infrared absorption[4] and laser-induced fluorescence spectroscopy.[1,2] Several kinetic studies involving HCCO have appeared recently, with total rate constant measurements reported for reactions with NO,[5−8] NO_2,[9,10] O_2,[11,12] H_2,[10] O,[13] and H.[14]

Emission of NO_x ($x = 1, 2$) by combustion processes is an important factor in the formation of urban smog, in which ozone and other photooxidants constitute a serious health hazard. Reducing smog formation by reducing the NO_x emissions has been an important requirement for modern technologies of hydrocarbon combustion. To date, some of the most efficient and universal solutions in the design of industrial combustion sources rely on fuel reburning technologies.[17−19] Innovative methods, such as fuel flexible reburning,[20] have been actively developed and optimized. The ketenyl radical (HCCO) is a significant one of the free radicals responsible for NO_x removal in the reburning processes.[21−25] Understanding the exact mechanism by which reactions of HCCO with NO_x act in NO_x scavenging is important for optimizing the efficiency of reburning technologies. The reaction of HCCO with NO, which acts as an efficient strategy of NO-removal, has been the subject of experimental and theoretical investigations[5−8,26,27] and the detailed mechanism has been well characterized.

In stationary-source hydrocarbon combustion, a large fraction of NO_x is in the form of NO so that reactions of small hydrocarbon radicals with this species usually dominate their NO_2 counterparts, particularly at high temperatures. The degree of participation of NO_2 in NO_x flame chemistry depends largely on the temperature-sensitive [NO_2]/[NO], which is controlled mainly by the reactions NO + HO_2 → NO_2 + OH, NO_2 + H → NO + OH, NO + H + M → HNO + M, and HNO + H → NO + H_2.[28] These reactions usually dictate that concentrations of NO_2 are significant at temperatures below about 1400 K. Thus in low-temperature and fuel-rich conditions (as are typical in NO_x-reburning) the HCCO radical reacted with NO_2 is expected to contribute to the overall NO_x chemistry.

In 1992, Temps et al.[9] measured the single-temperature determined rate constant of the reaction HCCO + NO_2 and obtained $k = (2.7 \pm 0.7) \times 10^{-11}$ cm^3 s^{-1} at 298 k. In 2003, Carl et al.[10] reported for the first time the absolute rate constant of this reaction over extended temperature ranges (293−769 K); $k(T) = ((2.3 \pm 0.4) \times 10^{-11} \exp(340 \pm 40)K/T)$ cm^3 s^{-1}. In their study, the rate constant of HCCO + NO_2 exhibits a negative temperature dependence similar to that of the HCCO + NO reaction, but the Arrhenius *A*-factor is 1.4 times larger than that of the HCCO + NO reaction, which indicates that the reaction of HCCO with NO_2 is very rapid and may play an important role in the fate of NO_2 pollutants during combustion processes. Unfortunately, to the our best of our knowledge, no further information on product channels and product distribu-

* Address correspondence to this author. Fax: +86-431-8945942. E-mail: zeshengli@mail.jlu.edu.cn.

10.1021/jp056558g CCC: $33.50
Published on Web 01/28/2006

tions is available for the HCCO + NO_2 reaction, although they may play important roles in the NO_x-involved sequential chain processes. In view of the potential importance and the rather limited information, a thorough theoretical study on the potential energy surface (PES) of the title reaction is therefore desirable. The main objectives of the present article are the following: (1) provide the elaborated isomerization and dissociation channels on the PES of $HCCONO_2$; (2) investigate the products of the title reactions to assist in further experimental identification; and (3) give a deep insight into the mechanism of the ketenyl-NO_2-combustion reaction.

2. Computational Methods

All calculations are carried out with the GAUSSIAN03 program packages.[29] The geometries of all the reactants, products, intermediates, and transition states are optimized by using the hybrid density functional B3LYP[30] method (the Becke's three parameter hybrid functional with the nonlocal correlation functional of Lee-Yang-Par) with the 6-311G-(d,p)[31−33] basis set. The stationary nature of structures is confirmed by harmonic vibrational frequency calculations, i.e., equilibrium species possess all real frequencies, whereas transition states possess one and only one imaginary frequency. The zero-point energy (ZPE) corrections are obtained at the same level of theory. To confirm that the transition states connect designated isomers or products, intrinsic reaction coordinate (IRC)[34] calculation is employed at the B3LYP/6-311G(d,p) level. To yield more accurate energetic information, higher level single-point energy calculations are carried out at the CCSD-(T)[35] level (coupled-cluster approach with single and double substitutions including a perturbative estimate of connected triple substitutions) with the same basis set (CCSD(T)/6-311G(d,p)) by using the B3LYP/6-311G(d,p) optimized geometries. Unless otherwise specified, the CCSD(T) single-point energies with inclusion of B3LYP zero-point energy (ZPE) corrections (simplified as CCSD(T)//B3LYP) are used in the following discussions. Meanwhile, for the most relevant species present on the feasible pathways, we performed single-point energy calculations at the CCSD(T) level with the larger basis set 6-311+G(2df,2p)[31−33,36] (CCSD(T)/6-311+G(2df,2p)) based on the B3LYP/6-311G(d,p) geometries.

3. Results and Discussion

For the title HCCO + NO_2 reaction, 46 intermediate isomers and 89 transition states in singlet are obtained at the B3LYP/6-311G(d,p) level. The optimized structures of stationary points as well as the corresponding experimental data[37,38] are depicted in Figure 1. The electronic states and harmonic vibrational frequencies including available experimental data[38,39] are given in Table 1. Note that the calculated geometries and frequencies are in good agreement with experimental results within 7% at the B3LYP/6-311G(d,p) level. Table 2 displays the relative energies including ZPE corrections of the stationary points at various levels with available experimental data[10,40] for comparison. For our discussion easier, the energy of reactants **R** is set to be zero for reference. For simplicity, only the most relevant products, isomers, and transition states are included in Figure 1 and Tables 1 and 2. The optimized structures of unfavorable isomers for HCCO + NO_2 reaction are presented in Figure S1 (Supporting Information).[41] To clarify the reaction mechanism, the most relevant pathways of the singlet PES for HCCO + NO_2 reaction are depicted in Figure 2. The unfavorable reaction channels are plotted in Figures S2−S7 (Supporting Information).[41] Moreover, to further test the reaction mechanism obtained at the CCSD(T)/6-311G(d,p)//B3LYP/6-311G(d,p) level, we performed additional CCSD(T)/6-311+G(2df,2p) single-point energy calculations for the most relevant species based on the B3LYP/6-311G(d,p) geometries. The comparison between the calculated results of two higher levels is made.

3.1. Initial Association. The HCCO radical has C_s symmetry and $^2A''$ electronic state. The calculated CC bond length lies between the typical C═C double bond and C≡C triple bond, while the CO bond is close to the typical C═O double bond. Then the radical HCCO has the resonant structure H−•C═C═O|| ↔ H−C≡C−O||• ("|" denotes the lone electron pair and "•" denotes the single electron). The former has more weight confirmed by B3LYP/6-311G(d,p) spin densities 0.736677 e on the C atom neighboring to H atom and 0.299138 e on the O atom. Therefore, the initial association with NO_2 mainly focuses on the C-site neighboring to H atom. Both singlet and triplet $HCCONO_2$ potential energy surfaces (PES) may be suggested for the radical−molecule reaction of HCCO + NO_2. On the singlet PES, we consider three possible attack pathways for the C (neighboring H) of HCCO at the NO_2 molecule, that is, middle-N attack, end-O attack, and side N−O π-bonding attack. The middle-N attack can lead to the very low-lying adduct $OCCHNO_2$ (**1**). We tried to locate the transition state from **R** to **1** at the B3LYP/6-311G(d,p) level, but with no success. The pointwise potential curves at the B3LYP/6-311G(d,p) level (as shown in Figure 3) are calculated to further confirm whether this process possesses a barrier. Figure 3 shows that the adduct **1** is formed as the C atom neighboring the H atom of HCCO and the middle N atom of NO_2 approach each other to interact on an attractive potential energy surface. We noticed that further full optimization of the minimum with a C−N distance of 1.4 Å, as presented in Figure 3, leads to **1** at the B3LYP/6-311G-(d,p) level. It is obvious that this addition process is a barrierless association. The association is expected to be fast and to play a significant role in the reaction kinetics. In our calculations, the isomers **11**^{a} (*trans*-) and **11**^{b} (*cis*-) with a formal O1C1C2HO2NO3 structure are located as two energy minima lying 49.4 and 50.2 kcal/mol below the reactants **R**, respectively. Yet, they has relatively short C2O2 and NO3 bond lengths of 1.377 and 1.149 Å for **11**^{a}, respectively, and 1.366 and 1.147 Å for **11**^{b}, respectively, and the internal O2N bond is as long as 1.548 and 1.595 Å for **11**^{a} and **11**^{b}, respectively. Then, isomers **11**^{a} and **11**^{b} are more like the adduct species between OCCHO and NO rather than the ones between OCCH and NO_2 at the terminal O-end. However, despite their low energy, the initial carbon (neighboring H)-to-oxygen approach to form isomer **11**^{a} or **11**^{b} may not be the desired favorable entrance channel because a considerable barrier should be overcome from **R** to **11**^{a} or **11**^{b} due to the extensive bond rearrangement (activating the short N═O double bond (1.195 Å) in NO_2 to form the long N−O weak bond in **11** (1.548 Å in **11**^{a}, 1.595 Å in **11**^{b})). Unfortunately, we cannot locate the transition state **TSR/11**^{a} or **TSR/11**^{b} despite many attempts. Alternatively, we calculate the dissociation curves of isomers **11**^{a} and **11**^{b} at the B3LYP/6-311G(d,p) level via pointwise optimization, as shown in Figure 4, parts a and b. We can clearly see that when the internal C2−O2 bond exceeds 2.0 and 2.4 Å, respectively, the total energy of *trans*-OCCHONO and *cis*-OCCHONO starts to become higher than that of the reactants **R** (HCCO + NO_2). Unfortunately, optimization of *trans*-OCCHONO and *cis*-OCCHONO with an internal C2−O2 bond longer than 4.0 and 4.1 Å, respectively, always meets with energy convergence problems. Because the *trans*-OCCHONO and *cis*-OCCHONO complexes with R(C2O2) = 4.0 and 4.1, respectively, are still

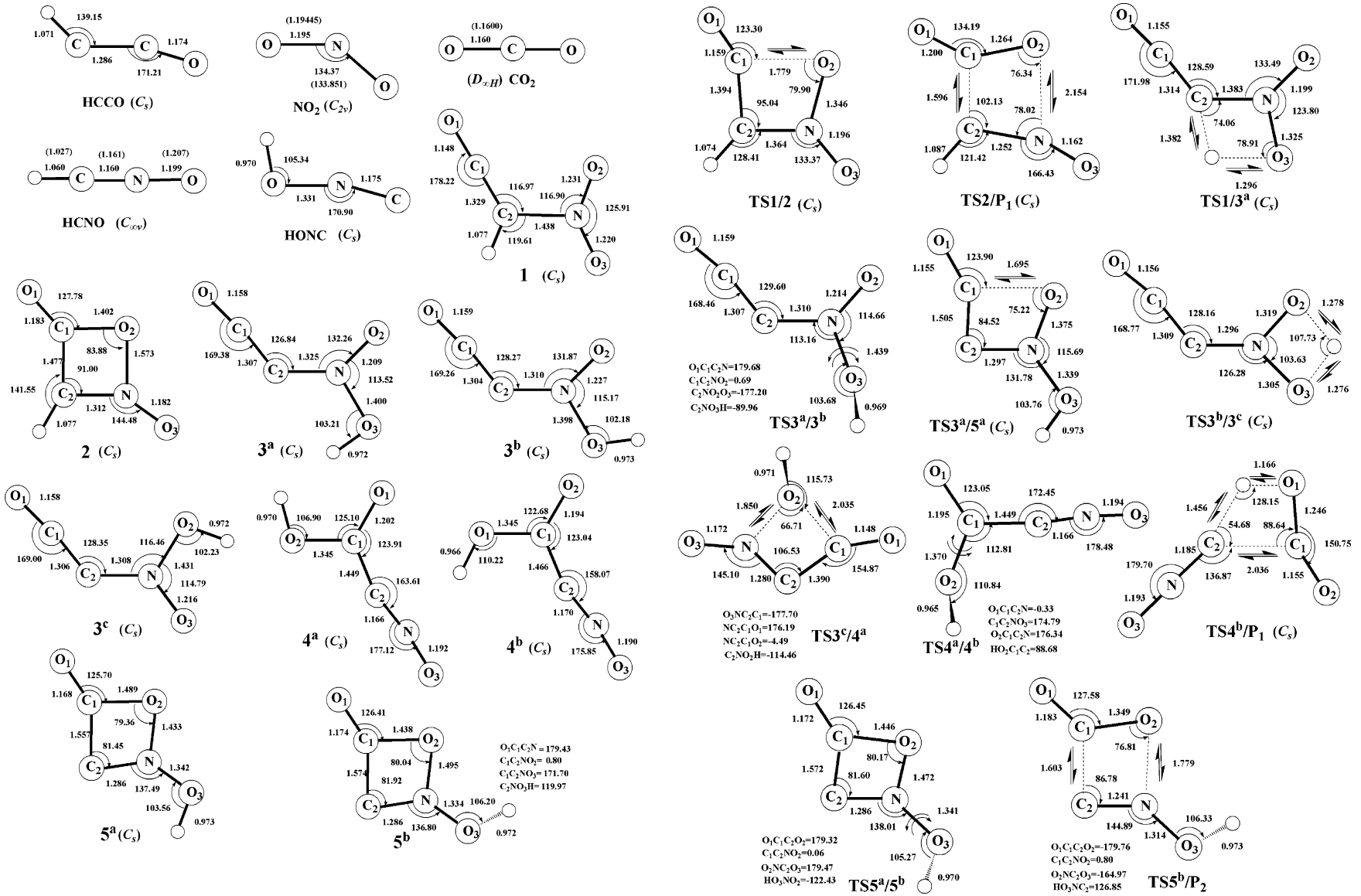

Figure 1. The B3LYP/6-311G(d,p) optimized geometries of reactants, the most relevant products, isomers, and transition states for the HCCO + NO_2 reaction. Bond distances are in angstroms and angles are in degrees. The values in parentheses are the experimental values (ref 37 for NO_2, ref 38 for HCNO and CO_2). In the transition states the direction of the imaginary frequency is indicated by "⇌".

TABLE 1: The Electronic States and Harmonic Vibrational Frequencies (cm^{-1}) of Reactants, Products, Isomers, and Transition States at the B3LYP/6-311G(d,p) Level

species	state	frequencies	exptl
HCCO	$^2A''$	439, 509, 565, 1269, 2093, 3354	382, 494, 564, 1037, 2024[b]
NO_2	$^2A^1$	767, 1399, 1707	750, 1318, 1618[a]
HCNO	$^1\Sigma$	244, 569, 571, 1300, 1334, 3513	224, 539, 567, 1232, 1254, 3338[b]
HONC	$^1A'$	257, 318, 980, 1408, 2207, 3735,	
CO_2	$^1\Sigma_g$	667, 667, 1375, 2436	667, −, 1333, 2349[a]
1	$^1A'$	110, 162, 429, 543, 543, 564, 749, 779, 994, 1115, 1362, 1365, 1603, 2254, 3262	
2	$^1A'$	185, 300, 464, 609, 612, 672, 717, 749, 928, 1039, 1266, 1306, 1823, 1983, 3277	
3[a]	$^1A'$	128, 139, 479, 489, 558, 602, 659, 703, 869, 1036, 1330, 1474, 1703, 2213, 3709	
3[b]	$^1A'$	134, 139, 462, 493, 552, 608, 640, 698, 858, 1058, 1319, 1470, 1725, 2217, 3711	
3[c]	$^1A'$	134, 135, 417, 514, 553, 604, 622, 685, 745, 1039, 1316, 1465, 1745, 2215, 3714	
4[a]	$^1A'$	80, 98, 458, 490, 550, 577, 584, 744, 759, 1157, 1328, 1506, 1807, 2419, 3754	
4[b]	$^1A'$	92, 94, 455, 478, 490, 550, 591, 720, 775, 1152, 1283, 1480, 1850, 2382, 3791	
5[a]	$^1A'$	163, 268, 318, 462, 500, 575, 650, 709, 885, 969, 1129, 1458, 1573, 2003, 3714	
5[b]		165, 253, 342, 392, 511, 571, 673, 707, 862, 988, 1113, 1367, 1584, 1978, 3701	
TS1/2	$^1A'$	362i, 175, 399, 563, 586, 644, 716, 757, 976, 1045, 1278, 1312, 1706, 2122, 3297	
TS1/3[a]	$^1A'$	1896i, 97, 146, 517, 563, 642, 683, 716, 914, 987, 1220, 1453, 1617, 2158, 2219	
TS2/P$_1$	$^1A'$	580i, 128, 257, 444, 477, 639, 671, 687, 770, 1107, 1212, 1306, 1840, 2059, 3154	
TS3[a]**/3**[b]		459i, 133, 140, 483, 547, 604, 630, 657, 822, 1011, 1323, 1435, 1701, 2209, 3759	
TS3[a]**/5**[a]	$^1A'$	386i, 162, 381, 390, 547, 553, 625, 685, 899, 990, 1173, 1459, 1571, 2073, 3713	
TS3[b]**/3**[c]	$^1A'$	1927i, 129, 140, 514, 561, 605, 642, 960, 1005, 1099, 1205, 1286, 1675, 2219, 2307	
TS3[c]**/4**[a]		505i, 150, 274, 457, 493, 561, 578, 630, 659, 841, 1024, 1319, 1891, 2160, 3747	
TS4[a]**/4**[b]		571i, 64, 91, 460, 486, 551, 561, 663, 784, 1086, 1176, 1475, 1816, 2419, 3815	
TS4[b]**/P**$_1$	$^1A'$	1693i, 60, 78, 262, 434, 532, 593, 609, 767, 982, 1257, 1365, 1827, 2226, 2229	
TS5[a]**/5**[b]		235i, 171, 338, 401, 527, 599, 669, 707, 871, 983, 1102, 1415, 1550, 1984, 3733	
TS5[b]**/P**$_2$		416i, 152, 298, 307, 389, 485, 679, 724, 801, 1015, 1144, 1383, 1707, 1921, 3686	

[a] Experimental values from ref 38. [b] Experimental values from ref 39.

45.9 and 32.6 kcal/mol higher than those of **R**, we can conclude that the association between HCCO and NO_2 at the O-site is a barrier-consumed process due to the strong repulsion from the lone-pair electrons of O in NO_2. Moreover, the single unpaired electron is mainly positioned at the internal N-site of NO_2. (N has much more spin density than O, i.e., 0.4489 and 0.2756, respectively, at the B3LYP/6-311G(d,p) level). Then, the HCCO radical may attack the N-site of NO_2 to form isomer **1** much more favorably than it will attack the O-site of NO_2 to form isomer **11**[a] or **11**[b]. Therefore, it is safe to exclude the entrance pathway of end-O attack for the reaction HCCO + NO_2. The optimization of the side N−O π-bonding attacking isomer usually leads to isomer **1** or (**11**[a], **11**[b]). On the triplet PES, the middle-N attack can form the triplet isomer $OCCHNO_2$ (^{3}**1**) (−1.1 kcal/mol) via the transition state ^{3}**TSR/1** with the much higher barrier of 15.5 kcal/mol. The end-O attack can be realized via two transition states (^{3}**TSRP**$_6$ and ^{3}**TSRP**$_6$′) with the barrier no less than 24.5 kcal/mol leading to product **P**$_6$ (OHCCO + NO) (−46.9 kcal/mol). We cannot locate either the isomer or the transition state associated with the side-NO π-bonding attack. In view of the much higher entrance barriers, the triplet pathways may contribute less to the HCCO + NO_2 reaction compared with the singlet pathways, and thus will not be further discussed. Note that the optimized structures of ^{3}**1**, ^{3}**TSR/1**, ^{3}**TSR/P**$_6$, and ^{3}**TSR/P**$_6$′ are also described in Figure S1 (Supporting Information)[41] for comparison. On the other hand, on the singlet PES, for the pathway of the O atom of the HCCO radical attacking on NO_2, the middle-N attack and end-O attack can form the two isomers $HCCONO_2$ (**23**) and HCCOONO (**24**), respectively. We tried to locate the transition states of the middle-N attack (**TSR/23**) and end-O attack (**TSR/24**), but failed. Isomers **23** and **24** lie 5.1 and 33.0 kcal/mol higher than the reactants **R**, respectively. Clearly, formation of **23** and **24** is energetically inaccessible. For side-NO π-bonding attack, we cannot find any isomers or transition states. On the triplet PES, despite numerous attempts, we did not succeed in locating any transition states or isomers for the pathway of the O atom of the HCCO radical attacking on NO_2. As a result, the carbon (neighboring H)-to-nitrogen approach forming isomer $OCCHNO_2$ **1** on the singlet PES is just the initial adduct step of all of the calculated pathways in our work. In the following discussions, we mainly

TABLE 2: The Relative Energies (kcal/mol) (with inclusion of the B3LYP/6-311G(d,p) zero-point energy (ZPE) corrections) of Reactants, Products, Isomers, and Transition States at Various Levels

species	B3LYP/ 6-311G(d,p)	CCSD(T)/ 6-311G(d,p)// B3LYP/ 6-311G(d,p)	CCSD(T)/ 6-311+G(2df,2p)// B3LYP/ 6-311G(d,p)	exptl[a]
R (HCCO + NO_2)	0.0	0.0	0.0	
$\mathbf{P}_1$ (HCNO + CO_2)	−98.5	−102.1	−104.2	−101.9
$\mathbf{P}_2$ (HONC + CO_2)	−79.5	−90.2	−89.6	−92.3
1	−51.3	−53.2	−57.3	
2	−45.9	−48.8	−54.7	
3[a]	−28.8	−27.1	−30.9	
3[b]	−29.1	−27.2	−31.2	
3[c]	−29.9	−28.1	−32.2	
4[a]	−82.8	−85.3	−89.7	
4[b]	−79.0	−81.5	−86.3	
5[a]	6.5	−2.9	−6.8	
5[b]	6.4	−2.5	−6.4	
TS1/2	−41.8	−41.5	−47.9	
TS1/3[a]	−6.5	−4.3	−8.2	
TS2/P$_1$	−39.8	−38.6	−43.2	
TS3[a]**/3**[b]	−22.5	−21.8	−25.3	
TS3[a]**/5**[a]	7.4	−1.1	−5.5	
TS3[b]**/3**[c]	−2.8	−0.9	−5.0	
TS3[c]**/4**[a]	−11.3	−10.7	−14.5	
TS4[a]**/4**[b]	−72.1	−74.4	−79.5	
TS4[b]**/P**$_1$	−39.8	−40.6	−42.7	
TS5[a]**/5**[b]	6.9	−2.4	−6.1	
TS5[b]**/P**$_2$	8.2	2.8	−1.1	

[a] Experimental values from refs 10 and 40.

discuss the formation pathways of various products proceeding via isomer **1**.

3.2. Isomerization and Dissociation Pathways. With the very large exothermicity released from the reactant **R**, the initially formed isomer $OCCHNO_2$ **1** can take various isomerization pathways followed by final decomposition. For clarity, we first discuss the former feasible pathways from isomer **1** (as shown in Figure 2). The initial adduct $OCCHNO_2$ (**1**) (C_s, $^1A'$) is a stable and branched chainlike isomer, 53.2 kcal/mol below the reactants. As shown in Figure 2, the ring closure of isomer **1** may proceed to a planar four-membered-ring intermediate O-cCCHN(O)O (**2**) (C_s, $^1A'$) via transition state **TS1/2** (C_s,$^1A'$) with the barrier height 11.7 kcal/mol. As seen in Figure 1, the **TS1/2** has a tight CCNO four-membered-ring structure, in which the length of the forming C−O bond is 1.779 Å. Subsequently, isomer **2** can easily lead to product $\mathbf{P}_1$ (HCNO + CO_2) via a cyclic elimination of CO_2 along with the formation of HCNO (i.e., **TS2/P**$_1$). Only a 10.2 kcal/mol barrier must be overcome for the process **2** → $\mathbf{P}_1$. The planar C1C2NO2 four-membered-ring structure **TS2/P**$_1$ (C_s, $^1A'$) is characterized by slightly elongated C1−C2 and N−O2 bonds and compressed C1−O2 and C2−N bonds. Such a multistep process can be described as

Path 1: $OCCHNO_2$ (**1**) → O-cCCHN(O)O (**2**) → HCNO + CO_2 ($\mathbf{P}_1$)

Isomer **1** can alternatively undergo a 1,3-hydrogen migration from the C2 atom to the O3 atom via the transition state **TS1/3**[a] (C_s, $^1A'$) to give the branched-chain isomer OCCNOHO (**3**[a]). **TS1/3**[a] surmounts a high barrier of 48.9 kcal/mol, entering a relatively shallow potential well. The **TS1/3**[a] may be viewed as tight four-membered ring species. The migrating hydrogen is 1.382 Å away from the origin (C2 atom) and 1.296 Å away from the migrating terminus (O3 atom). Intermediates **3**[a] (C_s, $^1A'$), **3**[b] (C_s, $^1A'$), and **3**[c] (C_s, $^1A'$) are cis and trans species in terms of the hydrogen atom. The interconversion between **3**[a] and **3**[b] takes place via a N−O single bond rotation transition state **TS3**[a]**/3**[b] with a low internal rotation barrier (5.3 kcal/mol above **3**[a]), while the interconversion between **3**[b] and **3**[c] is a 1,3-hydrogen migration process (**TS3**[b]**/3**[c]) with a high barrier (26.3 kcal/mol above **3**[b]). **TS3**[a]**/3**[b] has a branched-chain structure with a N−O single bond length of 1.439 Å. The six atoms O1, C1, C2, N, O2, and O3 are almost coplanar with the H atom nearly perpendicular to this plane, whereas the NO2HO3 four-membered ring on the plane is found in **TS3**[b]**/3**[c] (C_s, $^1A'$) with H−O2 and H−O3 distances of 1.278 and 1.276 Å, respectively. No transition state for the conversion of **3**[a] → **3**[c] was found. Subsequently, isomer **3**[c] can convert to the other branched-chain structure OCOHCNO **4**[a] via 1,3-migration of the OH group through **TS3**[c]**/4**[a] after clearing the barrier of 17.4 kcal/mol. The **TS3**[c]**/4**[a] presents a loose NCCO four-membered-ring structure with surpringly long N−O2 and C1−O2 distances of 1.850 and 2.035 Å, respectively. The intermediates **4**[a] (C_s, $^1A'$) and **4**[b] (C_s, $^1A'$) are cis and trans isomers (based on H atom) connected by the C1−O1 single bond rotation transition state **TS4**[a]**/4**[b] with a small internal rotation barrier of less than 10.9 kcal/mol. Then, isomer **4**[b] may take the C−C bond cleavage associated with a concerted H-shift to form product $\mathbf{P}_1$ (HCNO + CO_2) via the transition state **TS4**[b]**/P**$_1$ (C_s, $^1A'$). The dissociation barrier is 40.9 kcal/mol for **4**[b] → $\mathbf{P}_1$. The HO1C1C2 four-membered ring with planar structure is found in **TS4**[b]**/P**$_1$. The migrating hydrogen is 1.166 Å away from the origin (O1-atom) and 1.456 Å away from the migrating terminus (C2-atom), while the breaking C1−C2 bond length is surprisingly long at 2.036 Å. These processes can be written simply as

Path 2: $OCCHNO_2$ (**1**) → OCCNOHO (**3**[a], **3**[b], **3**[c]) → OCOHCNO (**4**[a], **4**[b]) → HCNO + CO_2 ($\mathbf{P}_1$)

In addition, isomer **3**[a] can also proceed via a ring-closure transition state **TS3**[a]**/5**[a] (C_s, $^1A'$) to form the four-membered-ring structure O-cCCN(OH)O **5**[a] (C_s, $^1A'$), which will readily convert to **5**[b] via the N−O3 bond rotation transition state **TS5**[a]**/5**[b]. The conversion barriers of **3**[a] → **5**[a] and **5**[a] → **5**[b] are 26.0 and 0.5 kcal/mol, respectively. The planar C1C2NO2 four-membered ring with the forming C1−O2 bond of 1.695 Å is found in **TS3**[a]**/5**[a]. The **TS5**[a]**/5**[b] also has the C1C2NO2 four-membered ring form, which is nearly planar, with an exocyclic N−O3 bond length of 1.341 Å. Whereafter, isomer **5**[b] can easily dissociate to $\mathbf{P}_2$ (HONC + CO_2) through the direct side CO_2-extrusion via the transition state **TS5**[b]**/P**$_2$ with a very small barrier of 5.3 kcal/mol. As shown in Figure 1, **TS5**[b]**/P**$_2$ presents a tight C1C2NO2 four-membered-ring structure, which is slightly nonplanar. The C1−C2 and N−O2 bonds that will be broken are 1.603 and 1.779 Å, respectively. The formation pathway of $\mathbf{P}_2$ (HONC + CO_2) is

Path 3: $OCCHNO_2$ (**1**) → OCCNOHO (**3**[a]) → O-cCCN(OH)O (**5**[a], **5**[b]) → HONC + CO_2 ($\mathbf{P}_2$)

Now we turn our attention to the unfavorable pathways (in Figures S2−S7, Supporting Information).[41] We can easily see that all channels leading to $\mathbf{P}_1$−$\mathbf{P}_9$ involve the high-energy transition states that lie significantly above reactants **R** and much higher than the rate-determining transition states in Paths 1−3. Therefore, all of them are kinetically much less feasible at low temperatures and cannot compete with Paths 1−3. For simplicity, the detailed discussions will not be given here.

3.3. Reaction Mechanism. From the above analysis, it is clear that the HCCO radical can barrierlessly react with NO_2 at

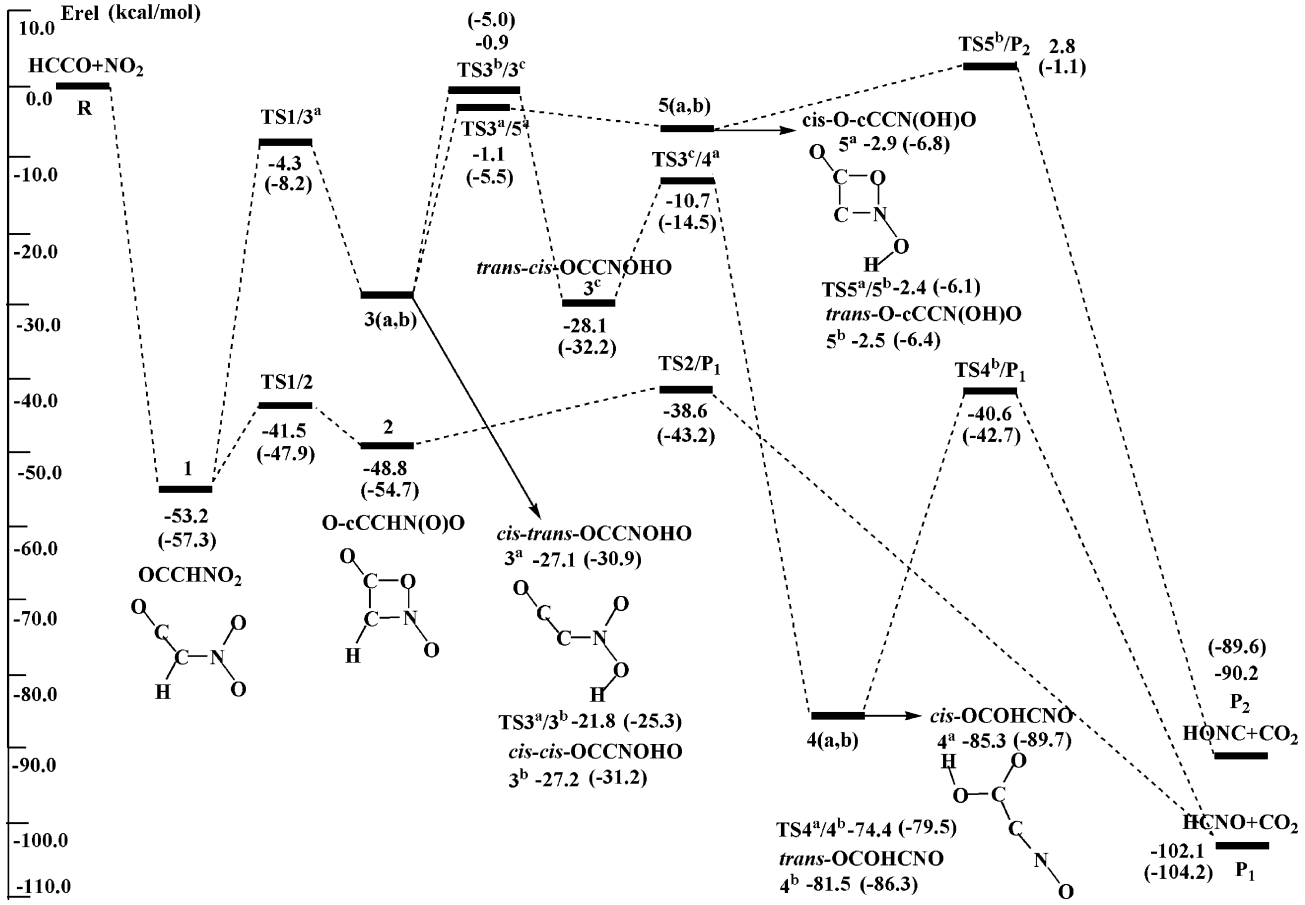

Figure 2. Schematic potential energy surface of the most relevant reaction pathways for the HCCO + NO_2 reaction in the singlet at the CCSD(T)/6-311G(d,p)//B3LYP/6-311G(d,p) + ZPE level. The values in parentheses are obtained at the CCSD(T)/6-311+G(2df,2p)//B3LYP/6-311G(d,p) + ZPE level. E_{rel} are relative energies (kcal/mol).

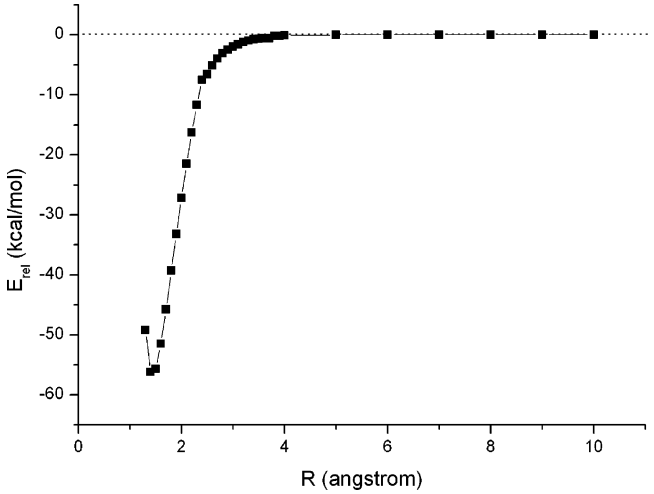

Figure 3. Potential energy curve for the formative process of the adduct $OCCHNO_2$ (**1**) at the B3LYP/6-311G(d,p) level. The calculations are performed by point-wise optimization of the other varied geometric parameters for every fixed internal C−N distance. The dotted line denotes the relative energy of the reactants **R** (HCCO + NO_2).

the middle-N site to form the low-lying isomer $OCCHNO_2$ **(1)**. Although there are various isomerization and dissociation channels starting from isomer **1**, only the former three pathways (Paths 1−3) are most probable. Among these pathways, Path 1 should be the most competitive pathway because the rate-determining transition state **TS2/P**$_1$ (−38.6 kcal/mol) in Path 1 lies much lower than **TS3**^{b}**/3**^{c} (−0.9 kcal/mol) in Path 2 and **TS5**^{b}**/P**$_2$ (2.8 kcal/mol) in Path 3. Furthermore, Path 3 is surely less competitive than Path 2 owing to the high-energy transition state **TS5**^{b}**/P**$_2$ above the reactants. However, since **TS5**^{b}**/P**$_2$ is just 2.8 kcal/mol higher than the reactants, Path 3 may become feasible at high temperatures. As a result, reflected in the final product distribution, we predict that product **P**$_1$ (HCNO + CO_2) (via Paths 1 and 2) is the most favorable product with predominant yields, while product **P**$_2$ (HONC + CO_2) (via Path 3) may have much less contribution and may play a role at high temperatures.

Because all the involved intermediates and transition states in the most competitive pathway Path 1 lie below the reactants **R**, the HCCO + NO_2 reaction is expected to be fast even at very low temperatures. It is worthy of pointing out that all the kinetically feasible pathways (Paths 1−3) of the title reaction can lead to innocuous species CO_2 and radicals HCNO and HONC that may further initiate many reactions in combustion chains[25,42−44] and that, most importantly, no nitrogen oxides are emitted on the singlet PES of the HCCO + NO_2 reaction, indicative of the very effective reduction of NO_2 by the HCCO radical. The reaction of HCCO + NO_2 is thus expected to significantly contribute to the elimination of nitrogen dioxide pollutants and it is therefore desirable to perform further kinetic investigations so as to thoroughly understand the HCCO + NO_2 reaction.

It is useful to make a comparison of the mechanism of the title reaction between the CCSD(T)/6-311G(d,p) and CCSD(T)/6-311+G(2df,2p) single-point levels based on B3LYP/6-311G(d,p) optimized geometries. It is readily found from Figure 2 that the features of PES obtained at the two levels are generally in parallel. (1) Path 1 may be the most feasible pathway; (2)

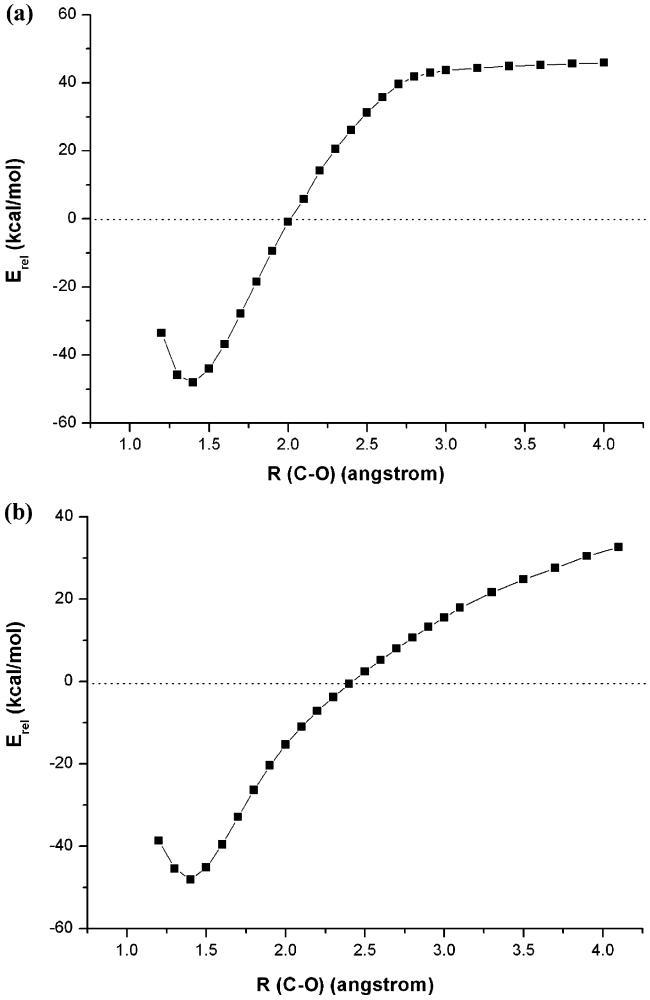

Figure 4. (a) Dissociation curve of the isomer *trans*-OCCHONO (**11**[a]) at the B3LYP/6-311G(d,p) level. (b) Dissociation curve of the isomer *cis*-OCCHONO (**11**[b]) at the B3LYP/6-311G(d,p) level. The calculations are performed by point-wise optimization of the other varied geometric parameters for every fixed internal C2−O2 distance. The dotted line denotes the relative energy of the reactants **R** (HCCO + NO_2).

Path 2 may be the much less competitive pathway; (3) Path 3 should be the least favorable pathway. It is known that the B3LYP method has been found to underestimate systematically the barrier heights;[45] thus, in the present study the energies are improved at the highly correlated CCSD(T) level. As shown by Table 2, our calculated relative energies at the higher CCSD(T)/6-311G(d,p) and CCSD(T)/6-311+G(2df,2p) levels agree well with the experimentally determined reaction heats[10,40] of products $\mathbf{P}_1$ (HCNO + CO_2) and $\mathbf{P}_2$ (HONC + CO_2) with the largest deviation of 2.28% and 2.26%, respectively. However, as can be seen from Table 2, the CCSD(T)/6-311+G(2df,2p) energies are about 5 kcal/mol lower than CCSD(T)/6-311G(d,p) energies in general. Additional sets of polarization (d and f) and diffuse (+) functions can increase the thermodynamic stability of the species relative to **R**. Thus, at the CCSD(T)/6-311+G(2df,2p) level, the process of *trans*-O-cCCN(OH)O (**5**[b]) dissociation to $\mathbf{P}_2$ (HONC + CO_2) via **TS5**[b]/$\mathbf{P}_2$ in Path 3 become kinetically feasible at low temperatures. However, Path 3 cannot compete with Path 1 and may be less competitive than Path 2, and is still of very minor importance. Thus, it is seen that in quality the reaction mechanism as well as the possible products are very similar at the two higher levels; we expect that the present CCSD(T)/6-311G(d,p)//B3LYP/6-311G(d,p) results could be reliable for the title reaction.

4. Conclusions

A detailed mechanistic study on the radical−radical reaction HCCO + NO_2 has been reported at the B3LYP and CCSD(T) (single-point) levels. The mechanism can generally be summarized as association, isomerization, and dissociation processes. (1) This reaction proceeds most likely through the singlet $HCCONO_2$ potential energy surface (PES) initiated by the carbon (neighboring to H atom)-to-nitrogen attack leading to adduct $OCCHNO_2$ (**1**) with no barrier. (2) The dominant decomposition pathway starting from **1** is Path 1 to give product HCNO + CO_2 ($\mathbf{P}_1$). The formation of product HONC + CO_2 ($\mathbf{P}_2$) may have a less comparable yield. The other reaction pathways are surely energetically unfeasible due to significant barriers. (3) The HCCO + NO_2 reaction may proceed very fast even at low temperatures and all favorable pathways can lead to unpolluted species CO_2. So the HCCO + NO_2 reaction may be suggested as an efficient de-NO_x strategy.

The calculated results presented here are expected to be useful for gaining insight into the mechanism of the title reaction that could be related to the NO_x combustion processes and to assist in further laboratory identification of the products.

Acknowledgment. This work is supported by the National Natural Science Foundation of China (20333050, 20303007), the Doctor Foundation by the Ministry of Education, the Foundation for University Key Teacher by the Ministry of Education, the Key Subject of Science and Technology by the Ministry of Education of China, and the Key subject of Science and Technology by Jilin Province.

Supporting Information Available: Figures showing B3LYP/6-311G(d,p) optimized geometries and potential energy surfaces of unfavorable reaction channels (ref 41). This material is available free of charge via the Internet at http://pubs.acs.org.

References and Notes

(1) Brock, L. R.; Mischler, B.; Rohlfing, E. A.; Bise, R. T.; Neumark, D. M. *J. Chem. Phys.* **1997**, *107*, 665.
(2) Brock, L. R.; Mischler, B.; Rohlfing, E. A. *J. Chem. Phys.* **1999**, *110*, 6773.
(3) Osborn, D. L.; Mordaunt, D. H.; Choi, H.; Bise, R. T.; Neumark, D. M.; Rohlfing, C. M. *J. Chem.* Phys. **1996**, *106*, 10087.
(4) Unfried, K. G.; Glass, G. P.; Curl, R. F. *Chem. Phys. Lett.* **1991**, *177*, 33.
(5) Boullart, W.; Ngugen, M. T.; Peeters, J. *J. Phys. Chem.* **1994**, *98*, 8036.
(6) Carl, S. A.; Sun, Q.; Vereecken, L.; Peeters, J. *J. Phys. Chem. A* **2002**, *106*, 12242.
(7) Rim, K. T.; Hershberger, J. F. *J. Phys. Chem. A* **2000**, *104*, 293.
(8) Meyer, J. P.; Hershberger, J. F. *J. Phys. Chem. B* **2005**, *109*, 8363.
(9) Temps, F.; Wagner, H. G.; Wolf, M. *Z. Phys. Chem.* (*Munich*) **1992**, *176*, 27.
(10) Carl, S. A.; Sun, Q.; Teugels, L.; Peeters, J. *Phys. Chem. Chem. Phys.* **2003**, *5*, 5424.
(11) Osborn, D. L. *J. Phys. Chem. A* **2003**, *107*, 3728.
(12) Carl, S. A.; Sun, Q.; Peeters, J. *J. Chem. Phys.* **2001**, *114*, 10332.
(13) Peeters, J.; Boullart, W.; Devriendt, K. *J. Phys. Chem.* **1995**, *99*, 3583.
(14) Glass, G. P.; Kumaran, S. S.; Michael, J. V. *J. Phys. Chem. A* **2000**, *104*, 8360.
(15) Vinckier, C.; Schaekers, M.; Peeters, J. *J. Phys. Chem.* **1985**, *89*, 508.
(16) Schmoltner, P. M.; Chu, P. M.; Lee, Y. T. *J. Chem. Phys.* **1989**, *91*, 5365.
(17) Wendt, J. O.; Sterling, C. V.; Matovich, M. A. *Proc. Combust. Inst.* **1973**, *14*, 897−904.
(18) Chen, S. L.; McCarthy, J. M.; Clark, W. D.; Heap, M. P.; Seeker, W. R.; Pershing, D. W. *Proc. Combust. Inst.* **1986**, *21*, 1159−1169.
(19) Glarborg, P.; Karll, B.; Pratapas, J. M. *Proceedings of the 19th World Gas Conference*; Milano, Italy, 1994 and references therein.

(20) Lissianski, V. V.; Ho, L.; Maly, P. M.; Pizeq, G.; Zamansky, V. M. *Proc. Combust. Inst.* **2002**, *29*, WIP Abstract 1-25-1432.

(21) Boullart, W.; Nguyen, M. T.; Peeters, J. *J. Phys. Chem.* **1994**, *98*, 8036.

(22) Stapf, D.; Lueckel, W. *Proc. Combust. Inst.* **1996**, *26*, 2083.

(23) Wendt, J. O. L.; Sterling, C. V.; Matovich, M. A. *Symp.* (*Int.*) *Combust.* [*Proc.*] **1973**, *14*, 897.

(24) Kilpinen, P.; Glarborg, P.; Hupa, M. *Ind. Eng. Chem. Res.* **1992**, *31*, 1477.

(25) Dagaut, P.; Luche, J.; Cathonnet, M. *Int. J. Chem. Kinet.* **2000**, *32*, 365.

(26) Tokmakov, I. V.; Moskaleva, L. V.; Paschenko, D. V.; Lin, M. C. *J. Phys. Chem. A* **2003**, *107*, 1066.

(27) Vereecken, L.; Sumathy, R.; Carl, S. A.; Peeters, J. *Chem. Phys. Lett.* **2001**, *344*, 400.

(28) Faravelli, T.; Frassoldati, A.; Ranzi, E. *Combust. Flame* **2003**, *132*, 188.

(29) Frisch, M. J.; Trucks, G. W.; Schlegel, H. B.; Scuseria, G. E.; Robb, M. A.; Cheeseman, J. R.; Montgomery, J. A., Jr.; Vreven, T.; Kudin, K. N.; Burant, J. C.; Millam, J. M.; Iyengar, S. S.; Tomasi, J.; Barone, V.; Mennucci, B.; Cossi, M.; Scalmani, G.; Rega, N.; Petersson, G. A.; Nakatsuji, H.; Hada, M.; Ehara, M.; Toyota, K.; Fukuda, R.; Hasegawa, J.; Ishida, M.; Nakajima, T.; Honda, Y.; Kitao, O.; Nakai, H.; Klene, M.; Li, X.; Knox, J. E.; Hratchian, H. P.; Cross, J. B.; Adamo, C.; Jaramillo, J.; Gomperts, R.; Stratmann, R. E.; Yazyev, O.; Austin, A. J.; Cammi, R.; Pomelli, C.; Ochterski, J. W.; Ayala, P. Y.; Morokuma, K.; Voth, G. A.; Salvador, P.; Dannenberg, J. J.; Zakrzewski, V. G.; Dapprich, S.; Daniels, A. D.; Strain, M. C.; Farkas, O.; Malick, D. K.; Rabuck, A. D.; Raghavachari, K.; Foresman, J. B.; Ortiz, J. V.; Cui, Q.; Baboul, A. G.; Clifford, S.; Cioslowski, J.; Stefanov, B. B.; Liu, G.; Liashenko, A.; Piskorz, P.; Komaromi, I.; Martin, R. L.; Fox, D. J.; Keith, T.; Al-Laham, M. A.; Peng, C. Y.; Nanayakkara, A.; Challacombe, M.; Gill, P. M. W.; Johnson, B.; Chen, W.; Wong, M. W.; Gonzalez, C.; Pople, J. A. *Gaussian 03*, Revision B.04; Gaussian, Inc.: Pittsburgh, PA, 2003.

(30) Becke, A. D. *J. Chem. Phys.* **1993**, *98*, 5648.

(31) McLean, A. D.; Chandler, G. S. *J. Chem. Phys.* **1980**, *72*, 5639.

(32) Krishnan, R.; Binkley, J. S.; Seeger, R.; Pople, J. A. *J. Chem. Phys.* **1980**, *72*, 650.

(33) Frisch, M. J.; Pople, J. A.; Binkley, J. S. Self-Consistent Molecular Orbital Methods 25: Supplementary Functions for Gaussian Basis Sets. *J. Chem. Phys.* **1984**, *80*, 3265.

(34) Gonzalez, C.; Schlegel, H. B. *J. Phys. Chem.* **1990**, *94*, 5523.

(35) Pople, J. A.; Head-Gordon, M.; Raghavachari, K. J. *J. Chem. Phys.* **1987**, *87*, 5968.

(36) Clark, T.; Chandrasekhar, J.; Spitznagel, G. W.; Schleyer, P. v. R. *J. Comput. Chem.* **1983**, *4*, 294.

(37) Kuchitsu, K. *Structure of Free Polyatomic Molecules Basic Data*; Springer-Verlag: Berlin, Germany, 1998.

(38) Lide, D. R. *CRC Handbook of Chemistry and Physics*, 79th ed.; CRC Press: New York, 1998.

(39) Jacox, M. E. In *NIST Chemistry WebBook*, NIST Standard Reference database. No. 69, March 2003 Release (http://www.webbook.nist.gov).

(40) Osborn, D. L.; Mordaunt, D. H.; Coi, H.; Bise, R. T.; Neumark, D. M.; Rohlfing, C. M. *J. Chem.* Phys. **1997**, *106*, 10087.

(41) The B3LYP/6-311G(d,p) optimized geometries of unfavorable isomers for the HCCO + NO_2 reaction are presented in Figure S1 (Supporting Information), in which the bond distances are in angstroms and angles are in degrees. The values in italics are for the triplet species. Schematic singlet potential energy surfaces (PESs) of the unfavorable reaction channels for the HCCO + NO_2 reaction at the CCSD(T)//B3LYP/6-311G(d,p) + ZPE level are described in Figures S2−S7 (Supporting Information) according to different primary dissociation products, where E_{rel} are the relative energies (kcal/mol). The products channels related to $\mathbf{P}_1$ (HCNO + CO_2) are shown in Figure S2, those related to $\mathbf{P}_2$ (HONC + CO_2) in Figure S3, those related to $\mathbf{P}_3$ (HOCNO + CO) and $\mathbf{P}_4$ (HN(O)CO + CO) in Figure S4, those related to $\mathbf{P}_5$ (HOCN + CO_2) in Figure S5, those related to $\mathbf{P}_6$ (HC(O)CO + NO) and $\mathbf{P}_7$ (HC(O)NO-*trans* + CO) in Figure S6, and those related to $\mathbf{P}_8$ (HC(O)NO-*cis* + CO) and $\mathbf{P}_9$ (HONCO + CO) in Figure S7.

(42) Dagaut, P.; Lecomte, F.; Chevailler, S.; Cathonnet, M. *Combust. Flame* **1999**, *119*, 494.

(43) Bowman, C. T. *Symp.* (*Int.*) *Combust.* [*Proc.*] **1992**, *24*, 859.

(44) Glarborg, P.; Alzueta, M. U.; Dam-Johansen, K.; Miller, J. A. *Combust. Flame* **1998**, *115*, 1.

(45) Lynch, J.; Fast, P. L.; Harris, M.; Truhlar, D. G. *J. Phys. Chem. A* **2002**, *104*, 4811.